ATLAS measurements of CP violation with beauty mesons

Radek Novotný
on behalf of the ATLAS collaboration

EPS-HEP 2021, Hamburg-DESY
July 26, 2021

- $B_s^0 \to J/\psi\phi$ is used to measure the CP-violating phase ϕ_s which is potentially sensitive to New Physics (NP)
- The CP violation occurs due to interference between a direct decay and a decay with $B_s^0 - \bar{B}_s^0$ mixing
- In the SM ϕ_s is related to the CKM elements and predicted with high precision
  $\phi_s \simeq 2\arg[-(V_{ts}V_{tb}^*)/(V_{cs}V_{cb}^*)] = -0.03696^{+0.00072}_{-0.00082}$ rad

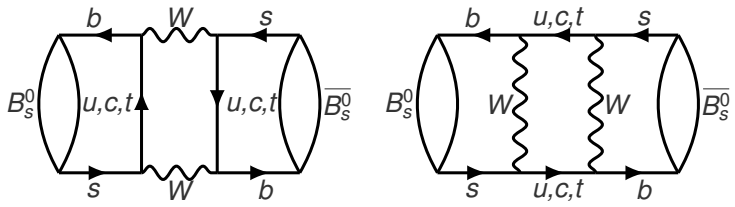

- The other quantity in B_s^0 mixing is $\Delta\Gamma_s = \Gamma_s^L - \Gamma_s^H$, where Γ_s^L and Γ_s^H are the decay widths of the different mass eigenstates. $\Delta\Gamma_s$ is not sensitive to New Physics, however the measurement is interesting to test the theory. The theory prediction is $\Delta\Gamma = (0.091 \pm 0.013)\,\text{ps}^{-1}$
- The New Physics processes could introduce additional contributions to the box diagrams describing the B_s^0 mixing

Status before LHC Run2

- The CP-violation measurement in the $B_s^0 \to J/\psi\phi$ channel was previously performed at the LHC in Run1 and at the Tevatron by the CDF and $D\emptyset$ experiments.
- The results were consistent with the SM prediction within measured uncertainties.
- Although large new physics enhancements of the mixing amplitude have been excluded by the precise measurement of the oscillation frequency, there is still room for improvements and discoveries

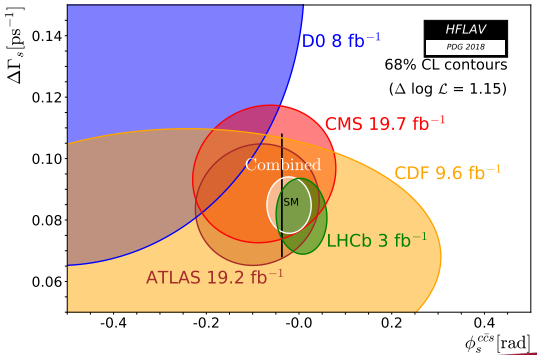

HFLAV Collaboration

ATLAS measurement in LHC Run2

Eur. Phys. J. C 81 (2021) 342

Data:

- pp collisions at $\sqrt{s} = 13\,\text{TeV}$ collected between years 2015 and 2017 corresponding to $80.5\,\text{fb}^{-1}$
- Statistically combined with Run1 ATLAS results:
  - $4.9\,\text{fb}^{-1}$ (7 TeV, pp 2011)
  - $14.3\,\text{fb}^{-1}$ (8 TeV, pp 2012)

Selection:

- Events collected with mixture of triggers based on $J/\psi \to \mu^+\mu^-$ identification, with muon p_T thresholds of either 4 GeV or 6 GeV (vary over run periods)
- Four-track vertex fit $\chi^2/\text{d.o.f.} < 3$
- Keep only the candidate with best vertex fit $\chi^2/\text{d.o.f.}$ in event
- $5150\,\text{MeV} < m(B_s^0) < 5650\,\text{MeV} \rightarrow$ in total 2 977 526 B_s^0 candidates

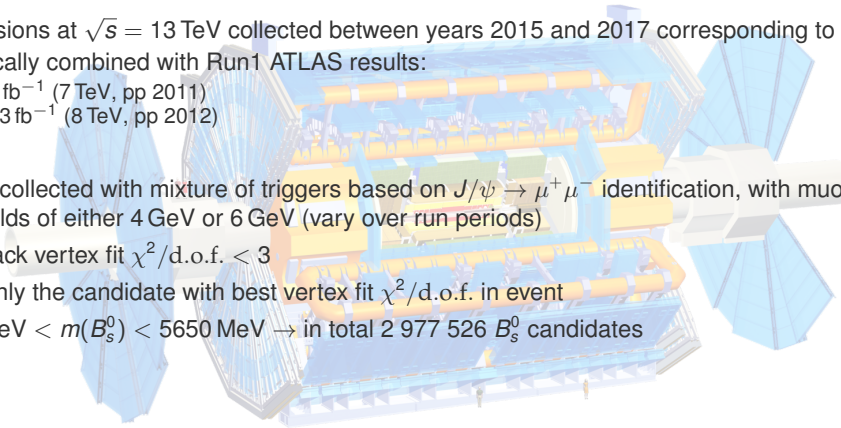

- $B_s^0 \to J/\psi\phi$ = pseudoscalar to vector-vector
- Final state: admixture of *CP*-odd ($L = 1$) and *CP*-even ($L = 0, 2$) states
- Distinguishable through time-dependent angular analysis
- Non-resonant *S*-wave decay $B_s^0 \to J/\psi K^+K^-$ contributes to the final state
- Included in the differential decay rate due to interference with the $B_s^0 \to J/\psi(\mu^+\mu^-)\phi(K^+K^-)$ decay

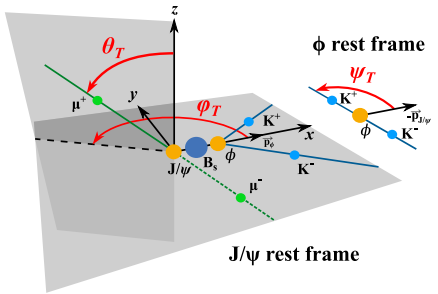

Figure: Angles between final state particles in transversity basis.

Mass-lifetime-angular fit

An unbinned maximum-likelihood fit is performed on the combined data samples extracting parameters of interest:

- CPV phase ϕ_s
- Decay widths: $\Delta\Gamma_s$, $\Gamma_s = \frac{\Gamma_L+\Gamma_H}{2}$
- The size of the CP-state amplitudes at $t = 0$: $|A_0(0)|^2$, $|A_\parallel(0)|^2$,$|A_\perp(0)|^2$, $|A_S(0)|^2$

$$|A_0(0)|^2 + |A_\parallel(0)|^2 + |A_\perp(0)|^2 = 1$$

- The strong phases $\delta_\parallel$, $\delta_\perp$, δ_S, $\delta_0 = 0$ (to avoid high correlations $\delta_S - \delta_\perp$ is measured)
- $\Delta m_s = |m_L - m_H|$ (value fixed to PDG $\Delta m_s = 17.77\,\text{ps}^{-1}$)
- $|\lambda| = 1.0$ (this analysis assumes no direct CP violation)

The likelihood function depends on:

- Base observables : m_i, t_i, $\Omega_i(\psi_{T_i}, \phi_{T_i}, \theta_{T_i})$
- Conditional observables per-candidate:
  - resolutions: σ_{m_i}, σ_{t_i} ($p_{\mathrm{T_i}}(B)$ dependent), $p_{\mathrm{T_i}}(B)$
  - tagging probability and method: $P(B|Q)$

Mass-lifetime-angular fit

$$\ln \mathcal{L} = \sum_{i=1}^{N} \{ \; \underbrace{w_i}_{\text{Tau weight}} \cdot \ln(\underbrace{f_s \cdot \mathcal{F}_s}_{\text{Signal}} + \underbrace{f_s \cdot f_{B_d^0} \cdot \mathcal{F}_{B_d^0} + f_s \cdot f_{\Lambda_b} \cdot \mathcal{F}_{\Lambda_b}}_{\text{Peaking background}} + \underbrace{(1 - f_s \cdot (1 + f_{B_d^0} + f_{\Lambda_b})) \cdot \mathcal{F}_{\text{bkg}}}_{\text{Combinatorial background}}) \}$$

- Data are corrected by the decay time correction
- Mass as well as lifetime use per-candidate width and scale factor, with flavour-dependent terms weighted by tagging probability $P(B|Q)$
- Contributions from $B_d^0 \to J/\psi K^{*0}$, $B_d^0 \to J/\psi K\pi$ and $\Lambda_b^0 \to J/\psi Kp$ due to wrong mass assignment (KK)
  - Efficiencies and acceptance from MC
  - BR from PDG
  - Fragmentation fractions from other measurements [1 – 5]
- Combinatorial background for angular distribution use Legendre polynomials from sidebands; fixed in the main fit

[1] LHCb-CONF-2013-011, 2013, [2] Phys. Rev. D 79 (2009) 112001, [3] JHEP 08 (2014) 143, [4] Chin. Phys. C 40 (2016) 011001, [5] Phys. Rev. Lett. 115 (2015) 072001

Flavour tagging

- Opposite side tagging
  - Use $b - \bar{b}$ pair correlation to infer initial signal flavour from the other B meson
  - Provide the probability of signal candidate to be B_s^0 or $\overline{B}_s^0$
- Opposite side tagging methods
  - Semileptonic
    - $b \to l$ transitions are clean tagging method
    - $b \to c \to l$ and neutral B-meson oscillations dilute the tagging results
  - Jet-Charge
    - Information from tracks in b-tagged jets
- Calibration using $B^{\pm} \to J/\psi K^{\pm}$
  - Self-tagging, non-oscillating channel
- Tagging methods used:
  - tight muon[1], electron, low-p_{T} muon[2], jet

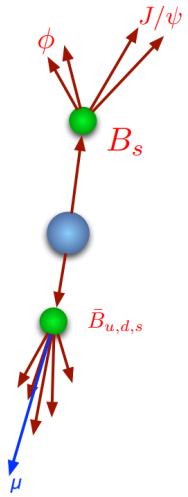

[1]Tight muon reconstruction is optimised to maximise the purity of muons at the cost of some efficiency.
[2]This working point is optimised to provide good muon reconstruction efficiency down to a p_{T} of $\approx 3\,\mathrm{GeV}$, while controlling the fake-muon rate.

- The probability to tag a B_s^0 meson as containing a $\bar{b}$-quark:

$$P(B|Q) = \frac{P(Q|B^+)}{P(Q|B^+) + P(Q|B^-)}$$

- **Efficiency**: Fraction of signals with specific tagger, $\varepsilon = \frac{N_{\text{tagged}}}{N_{\text{Bcand}}}$
- **Dilution**: $D = (1 - 2\omega)$, where ω is the mistag probability that is defined as ratio between the number of wrongly tagged events and the total number of tagged events
- **Tagging Power**: figure of merit of tagger performance
  - Depends on dilution and efficiency:

$$T = \varepsilon D^2 = \varepsilon(1 - 2\omega)^2$$

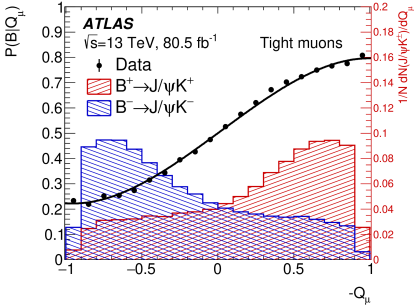

Tag method	ϵ_x [%]	D_x [%]	T_x [%]
Tight muon	4.50 ± 0.01	43.8 ± 0.2	0.862 ± 0.009
Electron	1.57 ± 0.01	41.8 ± 0.2	0.274 ± 0.004
Low-p_T muon	3.12 ± 0.01	29.9 ± 0.2	0.278 ± 0.006
Jet	12.04 ± 0.02	16.6 ± 0.1	0.334 ± 0.006
Total	21.23 ± 0.03	28.7 ± 0.1	1.75 ± 0.01

Systematic uncertainties

- Extensive systematic study was performed
- Here is the list of the major contributions to the total systematics:
  - **Flavour tagging:** calibration, $B_s^0 - B^{\pm}$ MC difference and dependencies on the pile-up distribution
  - **Fit bias:** fit stability is validated by the pseudo-experiments with default fit results
  - **Background angles model:** varying the bin boundaries, invariant mass window and sideband definition
  - **Best candidate selection:** statistically equivalent sample is created where all candidates in the event are retained
  - **Angular acceptance method:** different acceptance functions are calculated using different numbers of p_{T} bins as well as different widths and central values of the bins

- ATLAS found two well-separated local maxima of the likelihood for the strong-phases $\delta_\parallel$ and $\delta_\perp$

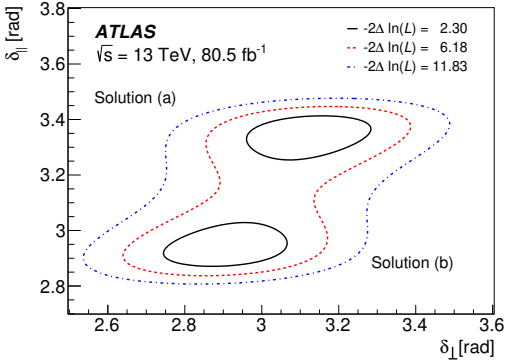

Parameter	Value	Statistical uncertainty	Systematic uncertainty
ϕ_s [rad]	−0.081	0.041	0.022
$\Delta\Gamma_s$ [ps^{-1}]	0.0607	0.0047	0.0043
Γ_s [ps^{-1}]	0.6687	0.0015	0.0022
$\lvert A_\parallel(0)\rvert^2$	0.2213	0.0019	0.0023
$\lvert A_0(0)\rvert^2$	0.5131	0.0013	0.0038
$\lvert A_S(0)\rvert^2$	0.0321	0.0033	0.0046
$\delta_\perp - \delta_S$ [rad]	−0.25	0.05	0.04
Solution (a)			
$\delta_\perp$ [rad]	3.12	0.11	0.06
$\delta_\parallel$ [rad]	3.35	0.05	0.09
Solution (b)			
$\delta_\perp$ [rad]	2.91	0.11	0.06
$\delta_\parallel$ [rad]	2.94	0.05	0.09

Combination with Run1 results

- The statistical combination of the new results with those obtained in Run1 was performed using the best linear unbiased estimator (BLUE) [6, 7] method. This method uses the measured values and uncertainties of the parameters as well as the correlations between them

$$\phi_s = -87 \pm 36(\text{stat.}) \pm 21(\text{syst.})\ \text{mrad},$$

$$\Delta\Gamma_s = 0.0657 \pm 0.0043(\text{stat.}) \pm 0.0037(\text{syst.})\ \text{ps}^{-1}$$

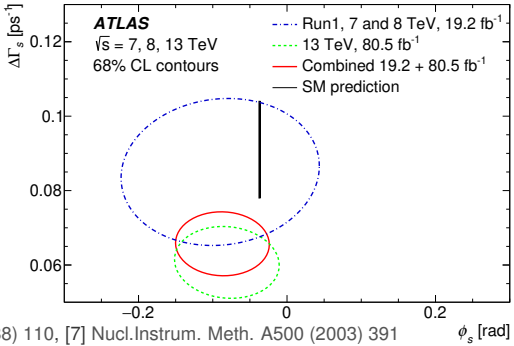

[6] Nucl. Instrum. Meth. A270 (1988) 110, [7] Nucl.Instrum. Meth. A500 (2003) 391

Comparison in $\Delta\Gamma_s - \phi_s$ plane

- Two-dimensional likelihood contours in the $\Delta\Gamma_s - \phi_s$ plane include the latest CMS [8] and LHCb [9] results from LHC Run2
- Experiments are consistent with each other and with the SM prediction, however some tension occurs in other parameters especially in Γ_s ($\sim 3\sigma$ tension)

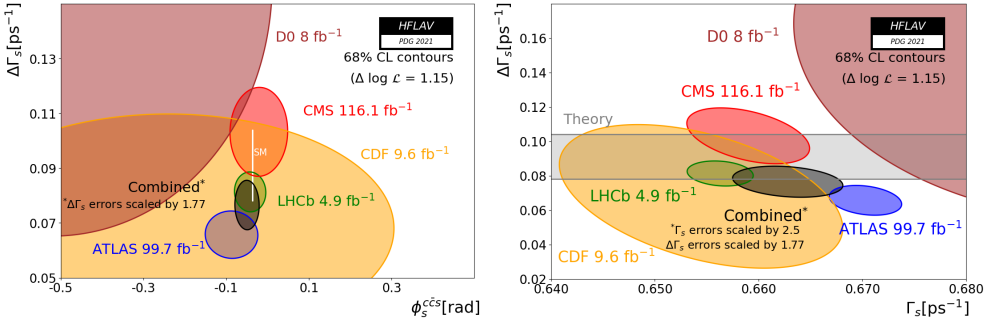

[8] Phys. Lett. B 816 (2021) 136188, [9] EPJC 80, 601 (2020)

Summary and outlook

- ATLAS performed analysis on the latest LHC Run2 data and the results were published in Eur. Phys. J. C 81 (2021) 342
- The results are consistent with the Run1 results and with SM predictions

- ATLAS is working on the full Run2 measurement (additional 60 fb^{-1} from 2018) with updated fit model that will include the extraction of Δm_s and $|\lambda|$ parameters

- Preparations for Run3 are very active, especially on the trigger side, to ensure a large amount of high quality data

Thanks for your attention!

ATLAS EXPERIMENT

Backup slides.

Time-Angular signal PDF

k	$O^{(k)}(t)$	$g^{(k)}(\theta_T, \psi_T, \phi_T)$
1	$\frac{1}{2}\lvert A_0(0)\rvert^2 \left[(1+\cos\phi_s)\,e^{-\Gamma_L^{(s)}t} + (1-\cos\phi_s)\,e^{-\Gamma_H^{(s)}t} \pm 2e^{-\Gamma_s t}\sin(\Delta m_s t)\sin\phi_s\right]$	$2\cos^2\psi_T(1-\sin^2\theta_T\cos^2\phi_T)$
2	$\frac{1}{2}\lvert A_\parallel(0)\rvert^2 \left[(1+\cos\phi_s)\,e^{-\Gamma_L^{(s)}t} + (1-\cos\phi_s)\,e^{-\Gamma_H^{(s)}t} \pm 2e^{-\Gamma_s t}\sin(\Delta m_s t)\sin\phi_s\right]$	$\sin^2\psi_T(1-\sin^2\theta_T\sin^2\phi_T)$
3	$\frac{1}{2}\lvert A_\perp(0)\rvert^2 \left[(1-\cos\phi_s)\,e^{-\Gamma_L^{(s)}t} + (1+\cos\phi_s)\,e^{-\Gamma_H^{(s)}t} \mp 2e^{-\Gamma_s t}\sin(\Delta m_s t)\sin\phi_s\right]$	$\sin^2\psi_T\sin^2\theta_T$
4	$\frac{1}{2}\lvert A_0(0)\rvert\lvert A_\parallel(0)\rvert\cos\delta_\parallel \left[(1+\cos\phi_s)\,e^{-\Gamma_L^{(s)}t} + (1-\cos\phi_s)\,e^{-\Gamma_H^{(s)}t} \pm 2e^{-\Gamma_s t}\sin(\Delta m_s t)\sin\phi_s\right]$	$\frac{1}{\sqrt{2}}\sin 2\psi_T\sin^2\theta_T\sin 2\phi_T$
5	$\lvert A_\parallel(0)\rvert\lvert A_\perp(0)\rvert \left[\frac{1}{2}(e^{-\Gamma_L^{(s)}t} - e^{-\Gamma_H^{(s)}t})\cos(\delta_\perp-\delta_\parallel)\sin\phi_s \pm e^{-\Gamma_s t}(\sin(\delta_\perp-\delta_\parallel)\cos(\Delta m_s t) - \cos(\delta_\perp-\delta_\parallel)\cos\phi_s\sin(\Delta m_s t))\right]$	$-\sin^2\psi_T\sin 2\theta_T\sin\phi_T$
6	$\lvert A_0(0)\rvert\lvert A_\perp(0)\rvert \left[\frac{1}{2}(e^{-\Gamma_L^{(s)}t} - e^{-\Gamma_H^{(s)}t})\cos\delta_\perp\sin\phi_s \pm e^{-\Gamma_s t}(\sin\delta_\perp\cos(\Delta m_s t) - \cos\delta_\perp\cos\phi_s\sin(\Delta m_s t))\right]$	$\frac{1}{\sqrt{2}}\sin 2\psi_T\sin 2\theta_T\cos\phi_T$
7	$\frac{1}{2}\lvert A_S(0)\rvert^2 \left[(1-\cos\phi_s)\,e^{-\Gamma_L^{(s)}t} + (1+\cos\phi_s)\,e^{-\Gamma_H^{(s)}t} \mp 2e^{-\Gamma_s t}\sin(\Delta m_s t)\sin\phi_s\right]$	$\frac{2}{3}\left(1-\sin^2\theta_T\cos^2\phi_T\right)$
8	$\alpha\lvert A_S(0)\rvert\lvert A_\parallel(0)\rvert \left[\frac{1}{2}(e^{-\Gamma_L^{(s)}t} - e^{-\Gamma_H^{(s)}t})\sin(\delta_\parallel-\delta_S)\sin\phi_s \pm e^{-\Gamma_s t}(\cos(\delta_\parallel-\delta_S)\cos(\Delta m_s t) - \sin(\delta_\parallel-\delta_S)\cos\phi_s\sin(\Delta m_s t))\right]$	$\frac{1}{3}\sqrt{6}\sin\psi_T\sin^2\theta_T\sin 2\phi_T$
9	$\frac{1}{2}\alpha\lvert A_S(0)\rvert\lvert A_\perp(0)\rvert\sin(\delta_\perp-\delta_S) \left[(1-\cos\phi_s)\,e^{-\Gamma_L^{(s)}t} + (1+\cos\phi_s)\,e^{-\Gamma_H^{(s)}t} \mp 2e^{-\Gamma_s t}\sin(\Delta m_s t)\sin\phi_s\right]$	$\frac{1}{3}\sqrt{6}\sin\psi_T\sin 2\theta_T\cos\phi_T$
10	$\alpha\lvert A_0(0)\rvert\lvert A_S(0)\rvert \left[\frac{1}{2}(e^{-\Gamma_H^{(s)}t} - e^{-\Gamma_L^{(s)}t})\sin\delta_S\sin\phi_s \pm e^{-\Gamma_s t}(\cos\delta_S\cos(\Delta m_s t) + \sin\delta_S\cos\phi_s\sin(\Delta m_s t))\right]$	$\frac{4}{3}\sqrt{3}\cos\psi_T\left(1-\sin^2\theta_T\cos^2\phi_T\right)$

Fit projections

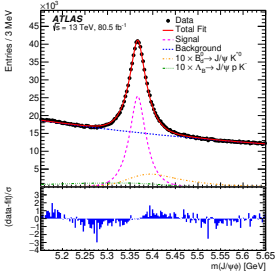

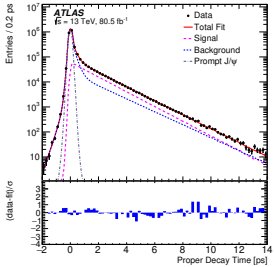

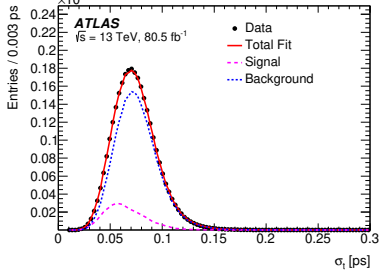

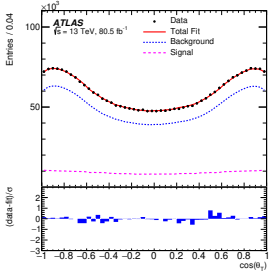

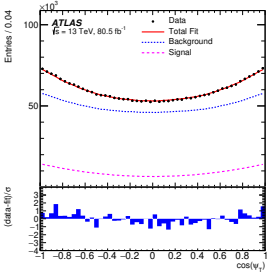

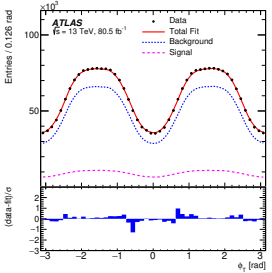

Systematic table

	ϕ_s [10^{-3} rad]	$\Delta\Gamma_s$ [10^{-3} ps^{-1}]	Γ_s [10^{-3} ps^{-1}]	$\lvert A_\parallel(0)\rvert^2$ [10^{-3}]	$\lvert A_0(0)\rvert^2$ [10^{-3}]	$\lvert A_S(0)\rvert^2$ [10^{-3}]	$\delta_\perp$ [10^{-3} rad]	$\delta_\parallel$ [10^{-3} rad]	$\delta_\perp - \delta_S$ [10^{-3} rad]
Tagging	19	0.4	0.3	0.2	0.2	1.1	17	19	2.3
ID alignment	0.8	0.2	0.5	< 0.1	< 0.1	< 0.1	11	7.2	< 0.1
Acceptance	0.5	0.3	< 0.1	1.0	0.9	2.9	37	64	8.6
Time efficiency	0.2	0.2	0.5	< 0.1	< 0.1	0.1	3.0	5.7	0.5
Best candidate selection	0.4	1.6	1.3	0.1	1.0	0.5	2.3	7.0	7.4
Background angles model:									
Choice of fit function	2.5	< 0.1	0.3	1.1	< 0.1	0.6	12	0.9	1.1
Choice of p_{T} bins	1.3	0.5	< 0.1	0.4	0.5	1.2	1.5	7.2	1.0
Choice of mass window	9.3	3.3	< 0.1	0.4	0.8	0.4	17	8.6	1.8
Choice of sidebands intervals	0.4	0.1	0.1	0.3	0.3	1.3	4.4	7.4	2.3
Dedicated backgrounds:									
B^0_d	2.6	1.1	< 0.1	0.2	3.1	1.5	10	23	2.1
Λ_b	1.6	0.3	0.2	0.5	1.2	1.8	14	30	0.8
Alternate Δm_s	1.0	< 0.1	< 0.1	< 0.1	< 0.1	< 0.1	15	4.0	< 0.1
Fit model:									
Time res. sig frac	1.4	1.1	0.5	0.5	0.6	0.8	12	30	0.4
Time res. p_{T} bins	0.7	0.5	0.8	0.1	0.1	0.1	2.2	14	0.7
S-wave phase	0.3	< 0.1	< 0.1	< 0.1	< 0.1	0.2	8.0	15	37
Fit bias	5.7	1.3	1.2	1.3	0.4	1.1	3.3	19	0.3
Total	22	4.3	2.2	2.3	3.8	4.6	55	88	39